ELSEVIER

Journal of Biomechanics 38 (2005) 1195–1204

JOURNAL OF BIOMECHANICS

www.elsevier.com/locate/jbiomech
www.JBiomech.com

A fibril-reinforced poroviscoelastic swelling model for articular cartilage

W. Wilson, C.C. van Donkelaar*, B. van Rietbergen, R. Huiskes

Department of Biomedical Engineering, EindhovenUniversity of Technology, Eindhoven, P.O. Box 513, 5600 MB, The Netherlands

Accepted 2 July 2004

Abstract

From a mechanical point of view, the most relevant components of articular cartilage are the tight and highly organized collagen network together with the charged proteoglycans. Due to the fixed charges of the proteoglycans, the cation concentration inside the tissue is higher than in the surrounding synovial fluid. This excess of ion particles leads to an osmotic pressure difference, which causes swelling of the tissue. The fibrillar collagen network resists straining and swelling pressures. This combination makes cartilage a unique, highly hydrated and pressurized tissue, enforced with a strained collagen network.

Many theories to explain articular cartilage behavior under loading, expressed in computational models that either include the swelling behavior or the properties of the anisotropic collagen structure, can be found in the literature. The most common tests used to determine the mechanical quality of articular cartilage are those of confined compression, unconfined compression, indentation and swelling. All theories currently available in the literature can explain the cartilage response occurring in some of the above tests, but none of them can explain these for all of the tests.

We hypothesized that a model including simultaneous mathematical descriptions of (1) the swelling properties due to the fixed-change densities of the proteoglycans and (2) the anisotropic viscoelastic collagen structure, can explain all these test simultaneously. To study this hypothesis we extended our fibril-reinforced poroviscoelastic finite element model with our biphasic swelling model. We have shown that the newly developed fibril-reinforced poroviscoelastic swelling (FPVES) model for articular cartilage can simultaneously account for the reaction force during swelling, confined compression, indentation and unconfined compression as well as the lateral deformation during unconfined compression. Using this theory it is possible to analyze the link between the collagen network and the swelling properties of articular cartilage.

Keywords: Cartilage; Biphasic; Triphasic; Collagen; Fiber reinforced; Finite element method

1. Introduction

Articular cartilage provides a low friction, wear resistant bearing surface in diarthrodial joints and distributes stresses to the underlying bone. From a mechanical point of view, the most relevant components of articular cartilage are the tight and highly organized collagen network together with the charged proteoglycans. Due to the fixed charges of the proteoglycans, the cation concentration inside the tissue is higher than in the surrounding synovial fluid. This excess of ion particles leads to an osmotic pressure difference, which causes swelling of the tissue (Urban et al., 1979). The fibrillar collagen network resists straining and swelling pressures (Mow et al., 1991). This combination makes cartilage a unique, highly hydrated and pressurized tissue, enforced with a strained collagen network.

Many theories to explain articular cartilage behavior under loading, expressed in computational models that either include the swelling behavior or the properties of the anisotropic collagen structure, can be found in the literature. Several models account for the swelling

*Corresponding author. Tel.: +31-40-247-3135; fax: +31 40-244-7355.

E-mail address: c.c.v.donkelaar@tue.nl (C.C. van Donkelaar).

0021-9290/$ - see front matter © 2004 Elsevier Ltd. All rights reserved.
doi:10.1016/j.jbiomech.2004.07.003

behavior of cartilaginous tissues (Lai et al., 1991; Huyghe and Janssen, 1997; Frijns et al., 1997; Sun et al., 1999; van Loon et al., 2003; Wilson et al., 2004a). These electro-mechanical models include three phases: an incompressible solid, an incompressible fluid and an ionic phase. Other models account for the collagen network (Li et al., 2000, 2002; Li and Herzog, 2004; Wilson et al., 2004b).

Two of these also include the viscoelastic behavior of the collagen fibrils (Li and Herzog, 2004; Wilson et al., 2004b). One model accounts for both the geometrically realistic collagen structure and its viscoelastic properties (Wilson et al., 2004b).

The most common tests used to determine the mechanical quality of articular cartilage are those of confined compression, unconfined compression, indentation and swelling. All theories described above can explain the cartilage response occurring in some of the above tests, but none of them can explain these for all of the tests. Obviously, models that do not account for the swelling behavior cannot explain swelling tests. Presently available swelling models are isotropic and homogeneous and can therefore not explain the results of indentation and unconfined compression tests accurately.

We hypothesized that a model including simultaneous mathematical descriptions of (1) the swelling properties due to the fixed-charge densities of the proteoglycans and (2) the anisotropic viscoelastic collagen structure, can explain all these test simultaneously. To study this hypothesis we extended our fibril-reinforced poroviscoelastic finite element model (Wilson et al., 2004b) with our biphasic swelling model (Wilson et al., 2004a). The unknown material properties of the new model were determined by fitting numerical data to experimental results of confined compression, unconfined compression, indentation and swelling tests on samples of bovine articular cartilage.

2. Methods

2.1. Constitutive model

Articular cartilage was assumed as biphasic (Mow et al., 1980). The solid matrix consists of a swelling non-fibrillar part representing the matrix, which contains mainly proteoglycans, and a fibrillar part representing the collagen network. Both the non-fibrillar and the fibrillar part of the solid matrix were included in one continuum element.

2.1.1. Fibrillar part

The 3D-collagen network was captured as a combination of large primary collagen fibrils and smaller secondary fibrils (Wilson et al., 2004b). As described in the arcade model of Benninghoff (1925), bundles of primary fibrils extend perpendicular from the subchondral bone, split up close to the articular surface into fibrils, which curve to a horizontal course, to flush with the articular surface. Each vertical bundle was assumed to split up in two different fibril directions, curving in radial direction (Fig. 1). It was assumed that the orientation of the secondary fibrils is random. To limit the computation time, the amount of secondary fibrils split off per material point was reduced to 7:3 running in the directions of the r-, θ- and z-axis, and 4 running in directions between those axes. Hence, the total number of fibrils in each material point is 9.

The viscoelastic behavior of the collagen fibrils was represented by a linear spring (with spring constant E_0), parallel to a non-linear spring (with spring constant $E_\varepsilon\varepsilon_f$) in series with a linear dashpot (with damping coefficient η) (Fig. 2).

Assuming that the fibrils only resist tension, the stresses in the viscoelastic fibrils are given by

$$\sigma_f = -\frac{\eta}{E_\varepsilon\varepsilon_f}\dot{\sigma}_f + E_0\varepsilon_f + \left(\frac{\eta E_0}{E_\varepsilon\varepsilon_f} + \eta\right)\dot{\varepsilon}_f \quad \text{for} \quad \varepsilon_f > 0,$$

$$\sigma_f = 0 \quad \text{for} \quad \varepsilon_f \leqslant 0, \tag{1}$$

where σ_f and ε_f are the fibril stress and strain, respectively. This differential equation was numerically integrated using an implicit backward Euler scheme. When the depth-dependent fibril density and the relative

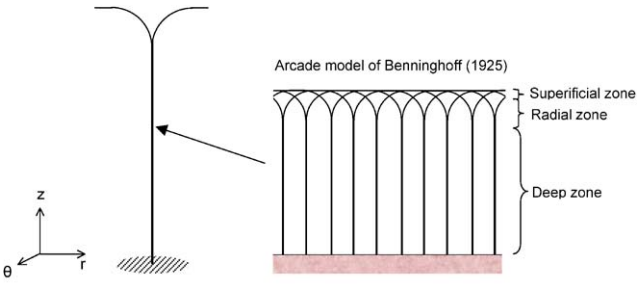

Fig. 1. Orientation of the primary fibrils as a function of depth. Right: cartoon of the arcade model of Benninghoff (1925). Left: Orientation of two primary collagen fibrils as implemented in the FEA model.

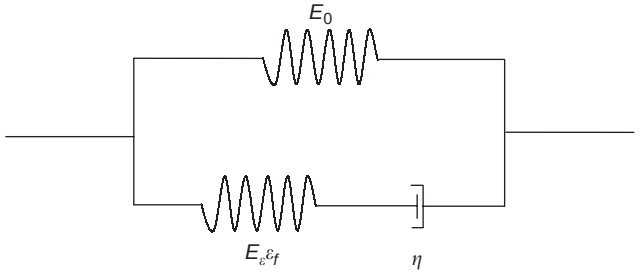

Fig. 2. Schematic model for the viscoelastic collagen fibrils.

amount of the primary compared to the secondary fibrils are taken into account, the stresses in the primary and secondary fibrils are given by

$$\sigma_{f,p} = \rho_z C \sigma_f \tag{2a}$$

and

$$\sigma_{f,s} = \rho_z \sigma_f, \tag{2b}$$

respectively. Here ρ_z is a factor accounting for fibril density (Wilson et al., 2004b) as a function of depth and C the amount of the primary fibrils with respect to the secondary fibrils. The stress–strain behavior of the collagen fibrils is illustrated in Fig. 3.

2.1.2. Non-fibrillar part

For the behavior of the non-fibrillar solid matrix a compressible neo-Hookean model was used (Wilson et al., 2004a),

$$\boldsymbol{\sigma}_{\text{non-fibrillar}} = K\frac{\ln(J)}{J}\mathbf{I} + \frac{G}{J}(\mathbf{F}\cdot\mathbf{F}^{\mathrm{T}} - J^{2/3}\mathbf{I}), \tag{3}$$

where J is the determinant of the deformation tensor $\mathbf{F}$. The bulk (K) and shear moduli (G) are defined as

$$K = \frac{E_m}{3(1-2\nu_m)}, \tag{4}$$

$$G = \frac{E_m}{2(1+\nu_m)}, \tag{5}$$

where E_m is the Young's modulus and ν_m the Poisson's ratio. The stress–strain behavior of the neo-Hookean model used is illustrated in Fig. 4. The hydraulic permeability (k) was assumed to be void ratio-dependent (Lai et al., 1981), and is given by (van der Voet, 1997)

$$k = k_0\left(\frac{1+e}{1+e_0}\right)^M \tag{6}$$

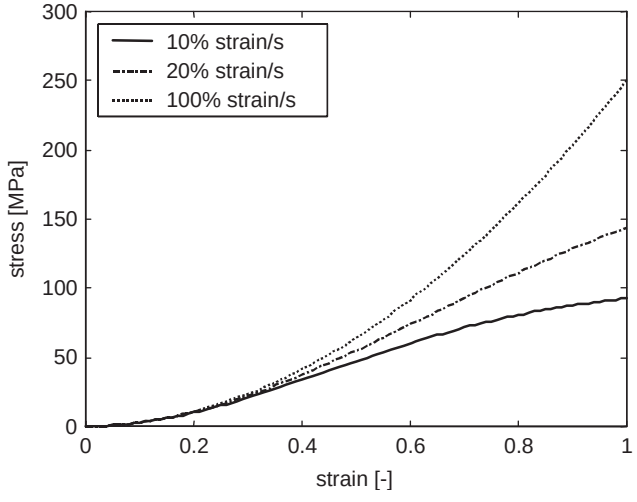

Fig. 3. Mechanical response of the viscoelastic collagen fibrils, for different strain rates ($E_0 = 1$ MPa, $E_\varepsilon = 500$ MPa, $\eta = 1000$).

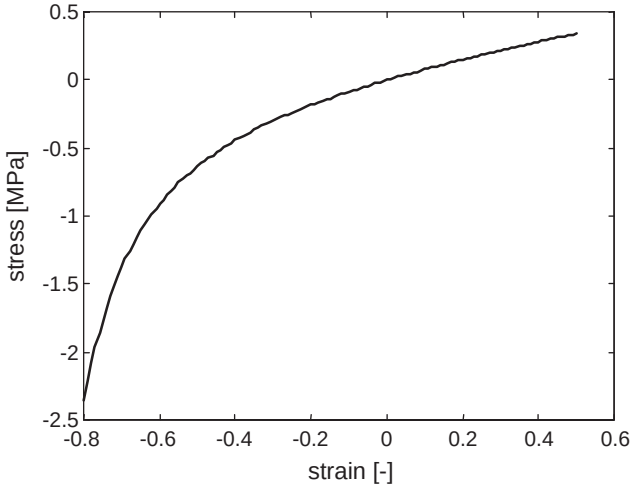

Fig. 4. Mechanical response of the compressible neo-Hookean model in confined compression ($E_m = 0.5$ MPa, $\nu = 0.1$).

with k_0 the initial permeability, M a positive constant, and e and e_0 the current and initial void ratios, respectively. The fluid fraction in equilibrium was assumed to be depth dependent (Lipshitz et al., 1975), as

$$n_{f,eq} = 0.85 - 0.15z^*, \tag{7}$$

where z^* is the normalized depth of the sample (0 at the articular surface and 1 at the cartilage bone interface).

2.1.3. Osmotic swelling

Owing to the fixed charges of the proteoglycans, the ion concentration in the articular cartilage is higher than in the surrounding synovial fluid. This excess of ion particles within the matrix creates a pressure gradient referred to as Donnan swelling pressure gradient, which is given by

$$\Delta\pi = \pi_{int} - \pi_{ext}, \tag{8}$$

where the internal (π_{int}) and external osmotic pressures (π_{ext}) are given by (Huyghe and Janssen, 1997)

$$\pi_{int} = \phi_{int} RT(c^+ + c^-), \tag{9a}$$

$$\pi_{ext} = \phi_{ext} RT(c^+_{ext} + c^+_{ext}) = 2\phi_{ext} RT c_{ext}, \tag{9b}$$

where R is the gas constant, T the absolute temperature, c^+ and c^- the concentrations of mobile cations and anions, and ϕ the osmotic coefficient. The equilibrium ion concentrations are given by (Huyghe and Janssen, 1997).

$$c^{\pm} = \frac{\pm c_F + \sqrt{c_F^2 + 4[(\gamma_{ext}{}^{\pm})^2/(\gamma_{int}^{\pm})^2]c_{ext}^2}}{2}, \tag{10}$$

where c_{ext} is the external salt concentration, c_F the fixed charge density and γ^α the activity coefficients. By substituting Eq. (10) into Eq. (9) the osmotic pressure

gradient in equilibrium becomes

$$\Delta\pi = \phi_{int} RT\left(\sqrt{c_F^2 + 4\frac{(\gamma_{ext}^{\pm})^2}{(\gamma_{int}^{\pm})^2}c_{ext}^2}\right) - 2\phi_{ext} RT c_{ext}. \tag{11}$$

The osmotic coefficient (ϕ^{α}) and activity coefficients (γ^{α}) are implemented as proposed by Huyghe et al. (2003). During all simulations T was 293 K and R was 8.3145 N mm/mmol. Based on literature data (Maroudas, 1968; Chen et al., 2001; Mankin et al., 2000) the equilibrium fixed charge density was assumed to be

$$c_{F,eq} = 0.11 + 0.09z^*. \tag{12}$$

2.1.4. Chemical expansion

Another type of swelling stress is due to chemical expansion, which is caused by the repulsion between large negative groups in the solid matrix. Lai et al. (1991) proposed for the chemical expansion stress

$$T_c = a_0 c_F \exp\left(-\kappa\frac{\gamma_{ext}^{\pm}}{\gamma_{int}^{\pm}}\sqrt{c^-(c^- + c_F)}\right) \tag{13}$$

with a_0 and κ material constants. The behavior of the osmotic swelling pressure and chemical expansion stress as a function of volumetric strain and external salt concentration is illustrated in Fig. 5.

2.2. Implementation

When assuming that the ion concentration is always in equilibrium (Lanir, 1987; Wilson et al., 2004a) the only variable in Eqs. (11) and (13) is the fixed charged density (c_F), which can be expressed as a function of the tissue deformation, as

$$c_F = c_{F,0}\left(\frac{n_{f,0}}{n_{f,0} - 1 + J}\right), \tag{14}$$

where $n_{f,0}$ is the initial fluid fraction and $c_{F,0}$ the initial fixed charge density. Since the osmotic pressure and chemical expansion stress in an equilibrium state are only functions of the deformation tensor $\mathbf{F}$, they can easily be implemented in a commercial finite element package (Wilson et al., 2004a).

At each integration point the total stress is given by the sum of the stresses in the non-fibrillar matrix and all fibril stresses, as

$$\boldsymbol{\sigma}_{\text{tot}} = \boldsymbol{\sigma}_{\text{non-fibrillar}} + \sum_{i=1}^{\text{totf}} \boldsymbol{\sigma}_{f,\text{global}}^{i} - \Delta\pi\mathbf{I} - T_c\mathbf{I} - \mu^f\mathbf{I}, \tag{15}$$

where μ^f is the chemical potential (Wilson et al., 2004a) and $\boldsymbol{\sigma}_{f,\text{global}}^{i}$ as in (Wilson et al., 2004b).

The model was implemented in ABAQUS v6.3 (Hibbitt, Karlsson & Sorensen, Inc., Pawtucket, RI, USA). An updated Lagrange procedure was used to account for geometric non-linearities. Details about the implementation can be found in earlier work of the authors, concerning the swelling part (Wilson et al., 2004a) and the fibril-reinforced part (Wilson et al., 2004b).

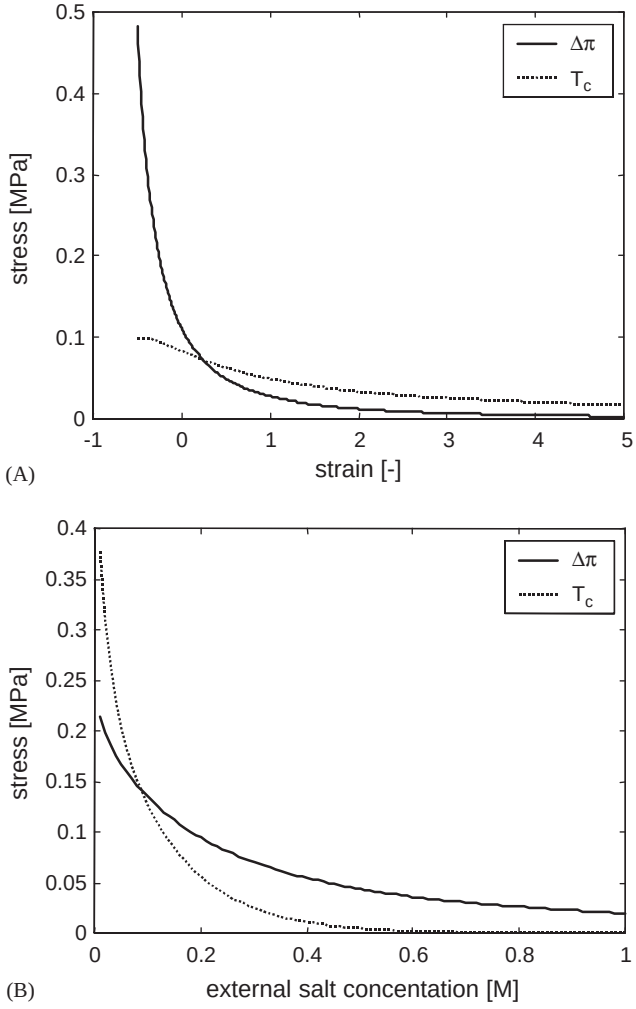

Fig. 5. (A) Osmotic pressure gradient ($\Delta\pi$) and chemical expansion stress as a function of volumetric strain ($c_0 = 0.15$) (B) Osmotic pressure gradient ($\Delta\pi$) and chemical expansion stress as a function of external salt concentration at zero strain ($T = 293$ K, $R = 8.3145$ N mm/mmol K, $c_0 = 0.15$ M, $c_F = 0.2$ meq/mm^3, $a_0 = 2.5$ MPa ml/meq, $\kappa = 9$ M^1).

2.3. Fundamental discrepancy between initial conditions in experiments and in models

Normal cartilage is in equilibrium with a physiological salt solution (0.15 M NaCl). The FEA always starts without swelling. Hence, the model has to equilibrate to a 0.15 M NaCl solution first. Since the material properties, like fluid fraction, fixed charge density, fibril orientation and cartilage thickness, are derived from measurements of cartilage in swollen equilibrium, the

initial material properties of the model must be estimated for which an initialization run is needed. In this case the model is allowed to equilibrate to an external salt solution (c_{ext}) of 0.15 M. We started with the equilibrium material properties as found in literature, and kept fluid fraction, fixed charge density, fibril orientation constant, by continuously resetting the parameters to their initial values after each iteration. The initial fluid fraction, fixed charge density, fibril orientation, sample height and initial void ratios were determined by

$$n_{f,0} = n_{f,eq}J - (J-1), \tag{16}$$

$$c_{F,0} = c_{F,eq}\left(\frac{n_{f,0} - 1 + J}{n_{f,0}}\right), \tag{17}$$

$$\vec{v}_{f,0} = \frac{\mathbf{F}^{-1}\cdot\vec{v}_{f,eq}}{\|\mathbf{F}^{-1}\cdot\vec{v}_{f,eq}\|}, \tag{18}$$

$$h_0 = \frac{h_{eq}}{(1+\varepsilon_z)}, \tag{19}$$

$$e_0 = \frac{n_{f,0}}{1-n_{f,0}}, \tag{20}$$

where $\vec{v}_{eq}$ is the fibrils orientation in equilibrium. Note that since the void ratios cannot be held constant in ABAQUS, the equilibrium void ratios in the initiation run are higher than the values computed from the equilibrium fluid fraction. Since the effect of the initial void ratio on the volume change is very small, the volume changes, and thereby changes in fluid fraction can be assumed correct. Hence, the computed initial material properties can also be assumed correct.

After determining the initial material properties with Eqs. (16)–(20), these properties are used as input for the actual simulation. Every calculation has to start with a step in which the model is allowed to equilibrate to an external salt solution of 0.15 M NaCl. It was determined that after this equilibrium the maximum error in equilibrium properties ($n_{f,eq}, c_{F,eq}, \vec{v}_{eq}, h_{eq}, e_{0,eq}$) compared to the desired values was less than 1%.

2.4. Determination of the material properties

The unknown material properties are $E_m, \nu_m, k_0, M, E_0, E_\varepsilon, \eta, C, a_0$ and κ. ν_m was assumed to be 0.01. E_m, a_0 and κ were determined by fitting them to a results of and 1D swelling experiment (Eisenberg and Grodzinsky, 1985) and the equilibrium response of a confined compression experiment (DiSilvestro and Suh, 2001). The properties $k_0, M, E_0, E_\varepsilon, \eta$ and C were subsequently determined by fitting them to the results of confined compression, unconfined compression and indentation experiments by DiSilvestro and Suh (2001).

The fitting procedures were performed iteratively, using a multidimensional unconstrained non-linear minimization procedure available in Matlab Version 5.3 (The MathWorks Inc., 1984–1999). From within this procedure ABAQUS was called to simulate the experiments. The reaction forces and lateral displacement (unconfined compression) were then transferred into Matlab. The confined compression, unconfined compression and indentation data were normalized in the same way as by DiSilvestro and Suh (2001). In order to be comparable with the single value for their lateral displacement, the lateral displacement from the unconfined compression test was averaged over the height of the sample. For determining the non-fibrillar material properties we used the objective function

$$f_1 = \frac{1}{n}\sum_{i=1}^{n}\left(\frac{F^i_{EXP,s} - F^i_{FEM,s}}{F^i_{EXP,s}}\right)^2 + \left(\frac{F_{EXP,c,eq} - F_{FEM,c,eq}}{F_{EXP,c,eq}}\right)^2, \tag{21}$$

and for determining the fibrillar material properties

$$f_2 = \frac{1}{n}\sum_{i=1}^{n}\left(\frac{F^i_{EXP,u} - F^i_{FEM,u}}{F^i_{EXP,u}}\right)^2 + \frac{1}{p}\sum_{k=1}^{p}\left(\frac{u^k_{EXP,u} - u^k_{FEM,u}}{u^k_{EXP,u}}\right)^2 + \frac{1}{m}\sum_{j=1}^{m}\left(\frac{F^j_{EXP,i} - F^j_{FEM,i}}{F^j_{EXP,i}}\right)^2 + \frac{1}{q}\sum_{l=1}^{q}\left(\frac{F^l_{EXP,c} - F^l_{FEM,c}}{F^l_{EXP,c}}\right)^2, \tag{22}$$

where $F_{EXP,\alpha}$ and $F_{FEM,\alpha}$ are the experimental and numerical reaction forces, $u_{EXP,\alpha}$ and $u_{FEM,\alpha}$ the experimental and numerical lateral displacements and n, m, and p are the number of data points. The subscripts s, c, u and i stand for swelling, confined compression, unconfined compression and indentation, respectively. Since the fibril properties influence the initial swelling computed, they might influence the fit of the non-fibrillar matrix properties. Therefore, two fitting processes were alternatingly repeated until no more changes in material parameters occurred.

2.5. Finite element modeling

2.5.1. 1D swelling

The swelling test was limited to a one-dimensional model, using an axisymmetric finite element mesh, consisting of a single column of 25 axisymmetric pore pressure elements (CAX4P) (Fig. 6). Since Eisenberg and Grodzinsky (1985) removed the top 2.5% and bottom 37.5% of their full thickness cartilage samples, we set the normalized depth z^* in Eqs. (7) and (12), from 0.025 to 0.625. The nodal displacements at the bottom plane were confined in z-direction. The displacements of all nodes were confined in radial direction. At the top of the model, zero pore pressure was prescribed, i.e. fluid can flow in and out freely. All other surfaces were assumed to be impermeable. The mesh was axially

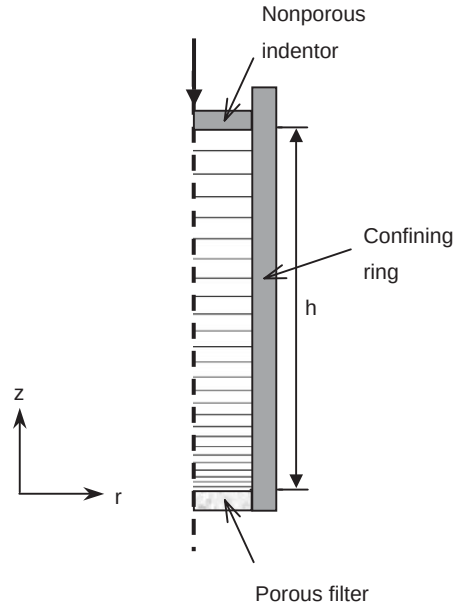

Fig. 6. 1D swelling mesh (h = 0.6 mm).

compressed by 15%. After full relaxation, the external salt concentration was decreased to 0.0001 M. After equilibrium was reached the salt concentration was increased to 0.05 M. After equilibrium the salt concentration was increased with 0.05 M. This process was repeated until an external salt concentration of 2 M was reached. During this process the height of the sample was held constant, while the axial reaction forces were computed.

2.5.2. Confined compression

For the confined compression test an axisymmetric finite element mesh was used, consisting of 380 linear axisymmetric pore pressure elements (CAX4P) (Fig. 7). The nodal displacements at the bottom plane were confined in z-direction. The displacements of the nodes at the symmetry axis were confined in radial direction. A rigid impermeable indentor with a radius of 1.46 mm was placed on top of the articular cartilage. At the nodes on the bottom plane and at the nodes in the top plane with do not lie under the indentor zero pore pressure was applied. The indentor was pushed down until 10% strain was reached. At the same time radial displacement of 0.045 mm was applied at the edge. After full relaxation, an additional 5% strain at a ramp strain rate of $0.001\,s^{-1}$ was applied. This strain was held constant until full relaxation occurred. While the additional 5% straining and relaxation occured, axial reaction forces were computed.

2.5.3. Unconfined compression

For the unconfined compression test an axisymmetric finite element mesh was used (Wilson et al., 2004b), consisting of 750 linear axisymmetric pore pressure

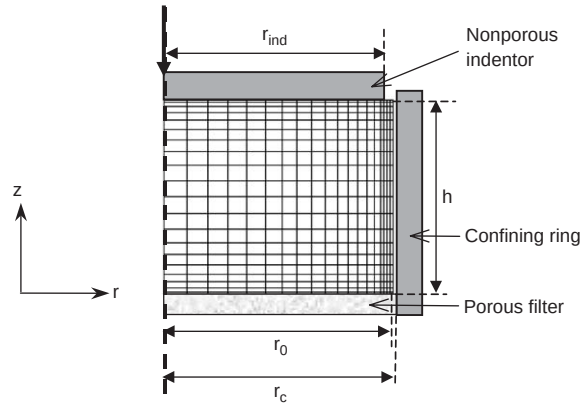

Fig. 7. Confined compression mesh ($r_0 = 1.5$ mm, $r_c = 1.545$ mm, $r_{ind} = 1.46$ mm, $h = 1.281$ mm). These dimensions were directly taken from DiSilvestro and Suh (2001).

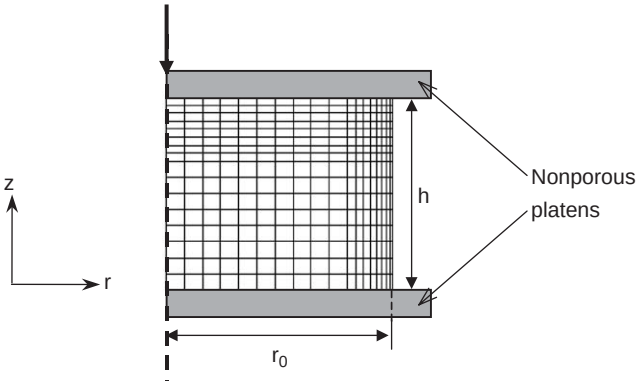

Fig. 8. Unconfined compression mesh ($r_0 = 1.5$ mm, $h = 1.281$ mm).

elements (CAX4P) (Fig. 8). The nodal displacements at the bottom plane were confined in z-direction. The displacements of the nodes at the symmetry axis were confined in radial direction. At $r = r_0$, zero pore pressure was prescribed, i.e. fluid can flow in and out freely. The mesh was axially compressed by 10%. After full relaxation, an additional 5% strain at a ramp strain rate of $0.001\,s^{-1}$ was applied. This strain was held constant until full relaxation occurred. While the additional 5% straining and relaxation occurred, axial reaction forces were computed.

2.5.4. Indentation

For simulation of the indentation test an axisymmetric finite element mesh was used (Wilson et al., 2004b), consisting of 600 linear axisymmetric pore pressure elements (CAX4P) (Fig. 9). The nodes at the bottom plane were confined in all directions. The displacements of the nodes at the symmetry-axis were confined in radial direction. At $z = h$, with $r_{ind} < r \leqslant 0$, zero pore pressure was prescribed. At the center, a rigid impermeable indentor with a radius of 1.53 mm was

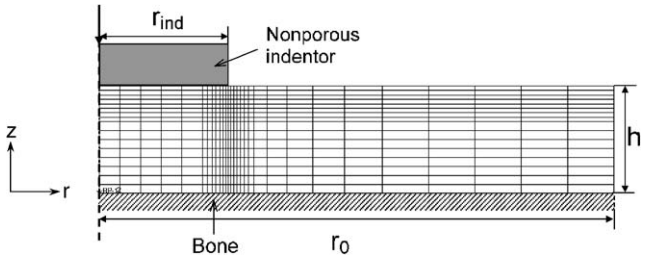

Fig. 9. Indentation mesh ($r_0 = 6.12$ mm, $r_{ind} = 1.53$ mm, $h = 1.281$ mm).

placed on top of the articular cartilage. The indentor was pushed down until 10% strain was reached. After full relaxation, an additional 5% strain at a ramp strain rate of $0.001\,s^{-1}$ was applied. This strain was held constant until full relaxation occurred. While the additional 5% straining and relaxation occurred, the axial reaction forces were computed.

3. Results

To determine the unknown material parameters of the fibril-reinforced poroviscoelastic swelling FEA model, reaction force and lateral displacements during 1D swelling, confined compression, unconfined compression and an indentation tests as computed with the model were fitted to the experimental data of DiSilvestro and Suh (2001) and Eisenberg and Grodzinsky (1985). The resulting fibril-reinforced poroviscoelastic swelling model parameters characterizing normal bovine articular cartilage were determined at $E_m = 0.3150$ MPa, $a_0 = 1.230$ MPa ml/meq, $\kappa = 11.26\,M^{-1}$, $k_0 = 1.522 \times 10^{-15}$ $m^4/N\,s$, $M = 5.661$, $E_0 = 2.737$ MPa, $E_\varepsilon = 340.5$ MPa, $\eta = 1643$ and $C = 3.009$.

For the 1D swelling test the normalized reaction force is almost in perfect agreement with the experimental data (Fig. 10). The coefficient of determination (R^2) of the 1D swelling test was 0.99.

For the first part of the loading curve of the confined compression test our model predicted a slightly higher reaction force than found in the experiments (Fig. 11). The coefficient of determination (R^2) of the confined compression test was 0.96.

For the unconfined compression test both the FEA reaction force and lateral displacement lie well within the experimental range found by DiSilvestro and Suh (2001) (Fig. 12). The reaction force was slightly lower during the relaxation part (Fig. 12A), while the lateral displacement was slightly greater during the loading part compared to the data of DiSilvestro and Suh (2001) (Fig. 12B). The coefficients of determination (R^2) were 0.96 and 0.87 for the reaction force and lateral displacement in unconfined compression, respectively.

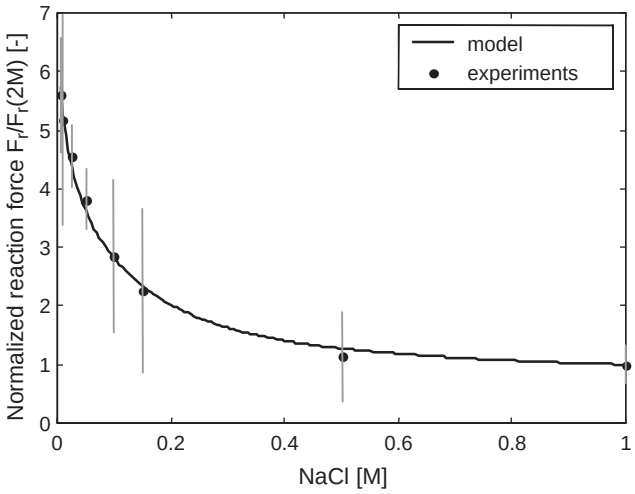

Fig. 10. Axial reaction force, normalized with the reaction force at an external salt concentration of 2 M, measured from 1D swelling tests (Eisenberg and Grodzinsky, 1985) along with reinforced curve fit.

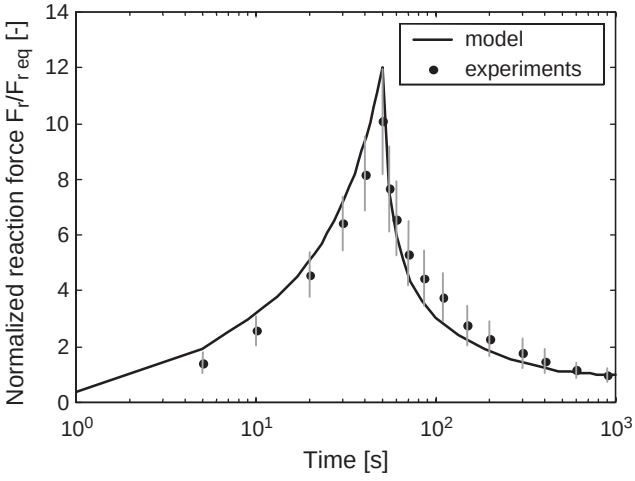

Fig. 11. Axial reaction force, normalized to equilibrium, measured from confined compression tests (DiSilvestro and Suh, 2001) along with model curve fit.

For the indentation test, the model described a delayed increase of the reaction force during the loading part (Fig. 13). The coefficient of determination (R^2) was 0.86 for the indentation test.

4. Discussion

The fibril-reinforced poroviscoelastic swelling (FPVES) model of articular cartilage presented in this paper incorporates the ultrastructural 3D architecture of the viscoelastic collagen network and the chemical and osmotic swelling behavior of articular cartilage. With this model the reaction force during 1D swelling,

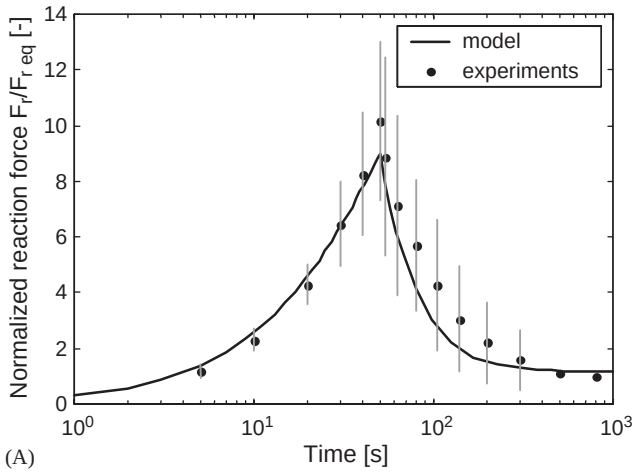

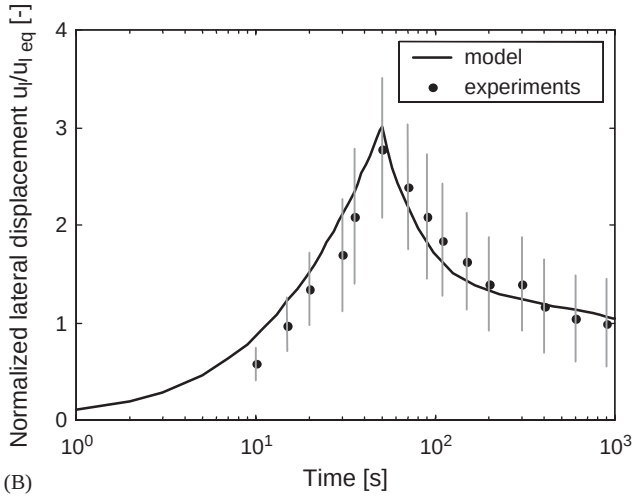

Fig. 12. (A) Axial reaction force, normalized to equilibrium, measured from unconfined compression tests (DiSilvestro and Suh, 2001) along with fibril reinforced model curve fit. (B) Lateral displacement, measured from unconfined compression tests (DiSilvestro and Suh, 2001) along with model curve fit.

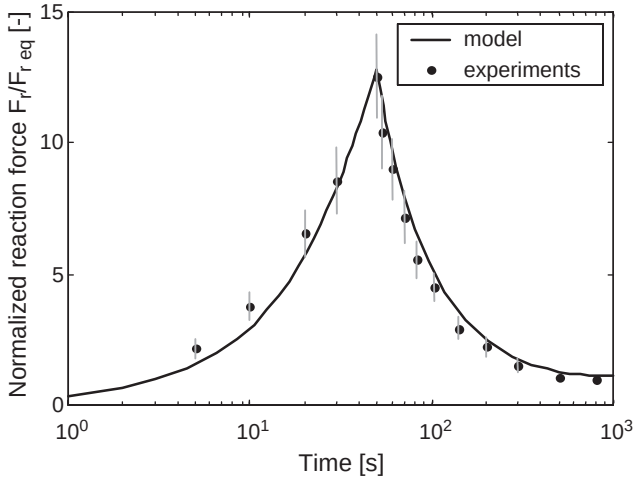

Fig. 13. Axial reaction force, normalized to equilibrium, measured from indentation tests (DiSilvestro and Suh, 2001) along with model curve fit.

confined compression, indentation and unconfined compression, as well as the lateral deformation during unconfined compression, could be accounted for simultaneously. Some of the required material properties were taken directly from the literature, while others were calculated from fits to published experimental data.

Since swelling pressures, included in our model, greatly contribute to the overall stiffness of the non-fibrillar matrix, the value found for Young's modulus of the non-fibrillar matrix was much lower than reported in the literature (DiSilvestro and Suh, 2001; Athanasiou et al., 1991). The values found for the constants a_0 and κ were in the same range as found by Lai et al. (1991). The value found for the permeability k_0 corresponded well with those found in the literature (Hasler et al., 1999). The confined compression test was very sensitive to the factor M. For values larger than 4 the reaction force (Fig. 10) peaked sharply. Since the confined compression test was not used in Wilson et al. (2004b) the value found for M in this paper is lower then found in (Wilson et al., 2004b) (2.402 instead of 7.081). The values found for E_0, E_ε, η and C were higher than previously found (Wilson et al., 2004b), because in this paper only seven secondary fibrils and two primary fibrils were included. The ratio between E_0 and E_ε was similar to the one found by Li et al. (2000, 2002) and Wilson et al. (2004b).

When fitting multiple material parameters the question is always whether a unique fit has been obtained. To ensure this, the fit was repeated several times with different initial parameters.

Although our model corresponds well with experimental data, there are slight differences. Essential parameters, including collagen content and orientation, fluid fraction and fixed charge density distribution were not measured in the same type of articular cartilage as cited in mechanical experiments used in this paper (DiSilvestro and Suh, 2001; Eisenberg and Grodzinsky, 1985). A possible mismatch may account for part of the differences between model and experimental data.

Although the samples used by Eisenberg and Grondzinksy and by DiSilvestro and Suh were both taken from mature 1–2 year old cattle, they were taken from different locations, the patellae-femoral groove and patellae, respectively. Since it is known that cartilage from different locations can have different mechanical properties (Hasler et al., 1999), this might also have caused a mismatch between the model and the experimental data.

In our model it was assumed that there are no internal stresses and strains when the cartilage is equilibrated in a hypertonic solution. At the beginning of our simulation we started with no swelling (hence, a stress-free state), and then let the model equilibrate to an external solution of 0.15 M, assuming that this provides an accurate and realistic representation of the initial mechanical conditions of the explant.

Although the collagen structure used is derived from experimental data (Benninghoff, 1925; Clark, 1985, 1991) it is a simplification relative to the actual one. In our current model, the primary fibril organization was based on the arcade model of Benninghoff (1925), which is valid in the central part of load bearing articular cartilage (Clark, 1985). However, the structure may vary between joints and the actual orientations in the samples tested were unknown.

In our model, the depth-dependent stiffness of the non-fibrillar matrix (Schinagl et al., 1997) was not explicitly taken into account. As shown by Chen et al. (2001), depth-dependent stiffness is mainly caused by depth-dependent swelling properties of the cartilage. Since depth-dependent swelling properties are incorporated in our model, we believe that the error due to the absence of depth-dependent matrix stiffness is small.

The viscoelastic and anisotropic properties of the biphasic non-fibrillar matrix (Mak, 1986) were also not included in this model. Although we anticipate that the major viscoelastic and anisotropic properties of the solid matrix come to the account of the fibrillar part, such properties of the non-fibrillar part may also explain part of the mismatches between the model and the experimental data.

We assumed that the ion flux is infinitely fast. We have previously shown that the effect of this simplification is relatively small (Wilson et al., 2004a). Nonetheless, it induces a small error. The model was fitted on data sets from different authors, who used different sources for their samples. The swelling experiment was performed on bovine femoropatellar groove cartilage (Eisenberg and Grodzinsky, 1985), while the tests by DiSilvestro and Suh (2001) were performed on bovine patellar cartilage. To minimize the influence the difference between the different types of cartilage, we normalized the swelling data.

Another possible cause for the small mismatches between the model the experimental data, could be a misinterpretation in the conductance of the confined compression experiment, as discussed by DiSilvestro and Suh (2001). We, however, believe that the influence of a possible inaccuracy of the experimental setup is not as large as suggested by DiSilvestro and Suh (2001), themselves. One of the reasons for them to believe that their confined compression results were incorrect, was the mismatch between their experimental data and their numerical model. Since an isotropic model cannot account for the behavior of articular cartilage in both confined and unconfined compression at the same time (Bursac et al., 1999), an anisotropic model, such as presented in this paper, is needed. Since the model of DiSilvestro and Suh (2001) did not include any anisotropy, their model is principally incapable of fitting these data simultaneously. This could, for a large part explain, the differences between their numerical and experimental results.

Huang et al. (2003) recently developed a biphasic-CLE-QLV model that includes both tension–compression non-linearity and the intrinsic viscoelasticity of the solid matrix. The main advantage of our model compared to the model of Huang et al. (2003) is that also the swelling behavior of the articular cartilage has been included. Furthermore, the current model enables the calculation of the stresses and strain in a realistic collagen structure.

Sun and Leong (2004) have recently developed a non-linear hyperelastic fiber-reinforced continuum mixture theory model that can account for tension–compression nonlinearity, osmotic swelling, pressurization, electrical potential and current, and water and ion transport as well as electroneutral nutrient transport. The main advantage of our model compared to the model of Sun and Leong, 2004 is that it is computationally less expensive and that it can account for large deformations. However, our model cannot account for electrical current and ion transport.

In conclusion, a new fibril-reinforced poroviscoelastic swelling (FPVES) model for articular cartilage was developed. This model includes the complex arcade structure of the collagen network, characteristic for articular cartilage, as well as the chemical and osmotic swelling properties of articular cartilage. We have shown that this model can appropriately fit confined compression, swelling, unconfined compression and indentation experiments with a single set of material parameters. Using this theory it is possible to analyze the link between the collagen network and the swelling properties of articular cartilage. This can be used to study cartilage physiology and pathology. Furthermore, the effect of loss of proteoglycans or collagen damage can be studied with this model. We believe that this model will be a useful tool for studies of mechanical behavior and damage mechanisms of articular cartilage.

References

Athanasiou, K.A., Rosenwasser, M.P., Buckwalter, J.A., Malinin, T.I., Mow, V.C., 1991. Interspecies comparisons of in situ intrinsic mechanical properties of distal femoral cartilage. Journal of Orthopaedic Research 9, 330–340.

Benninghoff, A., 1925. Form und Bau der Gelenkknorpel in ihren Beziehungen zur Funktion, Zeitschrift fue Zellforschvly, 2, 783–862.

Bursac, P.M., Obitz, T.W., Eisenberg, S.R., Stamenovic, D., 1999. Confined and unconfined stress relaxation of cartilage: appropriateness of a transversely isotropic analysis. Journal of Biomechanics 32 (10), 1125–1130.

Chen, S.S., Falcovitz, Y.H., Schneiderman, R., Maroudas, A., Sah, R.L., 2001. Depth-dependent compressive properties of normal aged human femoral head articular cartilage: relationship to fixed charge density. Osteoarthritis Cartilage 9 (6), 561–569.

Clark, J.M., 1985. The organization of collagen in cryofractured rabbit articular-cartilage—a scanning electron-microscopic study. Journal of Orthopaedic Research 3, 17–29.

Clark, J.M., 1991. Variation of collagen fibril alignment in a joint surface—a scanning electron-microscope study of the tibial plateau in dog, rabbit and man. Journal of Orthopaedic Research 9, 246–257.

DiSilvestro, M.R., Suh, J.K., 2001. A cross-validation of the biphasic poroviscoelastic model of articular cartilage in unconfined compression, indentation, and confined compression. Journal of Biomechanics 34, 19–525.

Eisenberg, S.R., Grodzinsky, A.J., 1985. Swelling of articular cartilage and other connective tissues: electromechanochemical forces. Journal of Orthopaedic Research 3 (2), 148–159.

Frijns, A.J.H., Huyghe, J.M., Janssen, J.D., 1997. A validation of the quadriphasic mixture theory for intervertebral disc tissue. International Journal of Engineering Science 35, 1419–1429.

Hasler, E.M., Herzog, W., Wu, J.Z., Muller, W., Wyss, U., 1999. Articular cartilage biomechanics: theoretical models, material properties, and biosynthesis response. Clinical Review in Biomechanical Engineering 27, 415–488.

Huang, C.Y., Soltz, M.A., Kopacz, M., Mow, V.C., Ateshian, G.A., 2003. Experimental verification of the roles of intrinsic matrix viscoelasticity and tension-compression non-linearity in the biphasic response of cartilage. Journal of Biomechanical Engineering 125 (1), 84–93.

Huyghe, J.M., Janssen, J.D., 1997. Quadriphasic theory of swelling incompressible porous media. International Journal of Engineering Science 35, 793–802.

Huyghe, J.M., Houben, G.B., Drost, M.R., van Donkelaar, C.C., 2003. An ionised/non-ionised dual porosity model of intervertebral disc tissue. Biomechanics and Modeling in Mechanobiology 2 (1), 3–19.

Lai, W.M., Mow, V.C., Roth, V., 1981. Effects of nonlinear strain-dependent permeability and rate of compression on the stress behavior of articular cartilage. Journal of Biomechanical Engineering 103, 61–66.

Lai, W.M., Hou, J.S., Mow, V.C., 1991. A triphasic theory for the swelling and deformation behaviours of articular cartilage. Journal of Biomechanical Engineering 113, 245–258.

Lanir, Y., 1987. Biorheology and fluid flux in swelling tissues. I. Bicomponent theory for small deformations, including concentration effects. Biorheology 24 (2), 173–187.

Li, L.P., Herzog, W., 2004. Strain-rate dependence of cartilage stiffness in unconfined compression: the role of fibril reinforcement versus tissue volume change in fluid pressurization. Journal of Biomechanics 37 (3), 375–382.

Li, L.P., Buschmann, M.D., Shirazi-Adl, A., 2000. A fibril reinforced nonhomogeneous poroelastic model for articular cartilage: inhomogeneous response in unconfined compression. Journal of Biomechanics 33, 1533–1541.

Li, L.P., Shirazi-Adl, A., Buschmann, M.D., 2002. Alterations in mechanical behaviour of articular cartilage due to changes in depth varying material properties—a nonhomogeneous poroelastic model study. Computer Methods in Biomechanics and Biomedical Engineering 5, 45–52.

Lipshitz, H., Etheridge, R., Glimcher, M.J., 1975. In vitro wear of articular cartilage. Journal of Bone and Joint Surgery 57, 527–537.

Mak, A.F., 1986. The apparent viscoelastic behavior of articular cartilage—the contributions from the intrinsic matrix viscoelasticity and interstitial fluid flows. Journal of Biomechanical Engineering 108, 123–130.

Mankin, H.J., Mow, V.C., Buckwalter, J.A., Iannotti, J.P., Ratcliffe, A., 2000. Articular cartilage structure, composition, and function. In: Buckwalter, J.A., Einhorn, T.A., Simon, S.R. (Eds.), Orthopaedic Basic Science: Biology and Biomechanics of the Musculoskeletal System. American Academy of Orthopaedic Surgeons Publishers, Rosemont, IL, pp. 47–92.

Maroudas, A., 1968. Physicochemical properties of cartilage in the light of ion exchange theory. Biophysical Journal 8 (5), 575–595.

Mow, V.C., Kuei, S.C., Lai, W.M., Armstrong, C.G., 1980. Biphasic creep and stress relaxation of articular cartilage in compression: theory and experiments. Journal of Biomechanical Engineering 102, 73–84.

Mow, V.C., Zhu, W., Ratclife, A., 1991. Structure and function of articular cartilage and meniscus. In: Mow, V.C., Hayes, W.C. (Eds.), Basic Orthopaedic Biomechanics. Raven Press, Ltd., New York, pp. 43–198.

Schinagl, R.M., Gurskis, D., Chen, A.C., Sah, R.L., 1997. Depth-dependent confined compression modulus of full-thickness bovine articular cartilage. Journal of Orthopaedic Research 15, 499–506.

Sun, D.D., Leong, K.W., 2004. A nonlinear hyperelastic mixture theory model for anisotropy, transport, and swelling of annulus fibrosus. Ann Biomed Eng. 32 (1), 92–102.

Sun, D.N., Gu, W.Y., Guo, X.E., Lai, W.M., Mow, V.C., 1999. A mixed finite element formulation of triphasic mechano-electrochemical theory for charged, hydrated biological soft tissues. International Journal for Numerical Methods in Engineering 45, 1375–1402.

Urban, J.P.G., Maroudas, A., Bayliss, M.T., Dillon, J., 1979. Swelling pressures of proteoglycans at the concentrations found in cartilagenous tissues. Biorheology 16, 447–464.

van der Voet, A., 1997. A comparison of finite element codes for the solution of biphasic poroelastic problems. Proceedings of the Institution of Mechanical Engineering [H] 211, 209–211.

van Loon, R., Huyghe, J.M.R.J., Wijlaars, M.W., Baaijens, F.P.T., 2003. 3D FE implementation of an incompressible quadriphasic mixture model. International Journal for Numerical Methods in Engineering 57 (9), 1243–1258.

Wilson, W., van Donkelaar, C.C., Huyghe, J.M., 2004a. A comparison between mechanoelectrochemical and biphasic swelling theories for soft hydrated tissues. Journal of Biomechanical Engineering, accepted

Wilson, W., van Donkelaar, C.C., van Rietbergen, C., Ito, K., Huiskes, R., 2004b. Stresses in the local collagen network of articular cartilage: a poroviscoelastic fibril-reinforced finite element study. Journal of Biomechanics 37 (3), 357–366.